RELAXATION OF A QUBIT COUPLED TO A FULLERENE MOLECULE

RELAXATION OF A TWO-LEVEL SYSTEM COUPLED TO A FULLERENE MOLECULE

By

KIRI NICHOL, B.Sc

A Thesis
Submitted to the School of Graduate Studies
in Partial Fulfillment of the Requirements
for the Degree
M.Sc

McMaster University

M.SC (2006)
(Physics)

McMaster University
Hamilton, Ontario

TITLE: Relaxation of a two-level system coupled to a fullerene molecule

AUTHOR: Kiri Nichol, B.Sc (University of British Columbia)

SUPERVISOR: Dr. A.J. Berlinsky and Dr. C. Kallin

NUMBER OF PAGES: v, 46

Abstract

Insight into many-body problems in quantum mechanics may be developed by solving simple models exactly using computational methods. The small size of endohedral-doped fullerene molecules allows the electronic states to be evaluated numerically using a spin model such as the Heisenberg Hamiltonian. The Lanczos algorithm is deployed to compute a few low-energy states of fullerene systems.

Since the spin of the dopant electrons can be manipulated using external magnetic fields, the system can be used as a qubit. For sufficiently large couplings between the dopant and the fullerene, the qubit may relax by releasing energy into the carbon cage. The resulting oscillations of the qubit are found to include a high frequency component introduced when the spin accesses multiple states with different energies. The frequency and the amplitude of the qubit's oscillations also depend on the magnitude of external fields and the size of the coupling between the dopant and the fullerene.

Contents

Chapter 1

Introduction

Many-body problems are of enduring interest because the characteristics of real systems depend extensively on interactions between a large number of particles. Taken as an ensemble, aggregations of particles exhibit collective properties which cannot be deduced from the behaviour of a few isolated components. While the behaviour of one or two particles can be well-described, the features of many-body systems have remained difficult to study because the interactions between a large number of constituent components give rise to complex behaviours.

Analytical techniques - such as perturbation theory and mean field approximations - allow study of many-body problems; however, the most curious behaviours are often masked by such simplifications. For example, the Bardeen-Cooper-Schrieffer theory of superconductivity cannot be derived through perturbative methods.

Computational techniques which allow the exact solution of many-body problems are an alternative to analytical methods provided the dimension of the Hamiltonian does not exceed memory restrictions. The size of the problem which can be tackled can often be increased by invoking clever storage schemes for sparse matrices and by using approximate diagonalization techniques which solve for a few interesting eigenvectors. "Toy" models, in which the interactions between components are simplified, allow larger systems to be

investigated and may allow insight into non-trivial effects due to large numbers of particles. One problem which numerical methods are especially suited to is the computation of electronic states of endohedral doped fullerenes - single atoms trapped inside a carbon cage. The number of atoms is small enough that numerical methods may be deployed to generate a few exact low-energy states using a simple spin model such as the Heisenberg Hamiltonian.

1.1 Quantum computing with endohedral fullerenes

The unusual structural and electronic properties of carbon fullerene compounds have inspired the development of nanoscale devices for many novel applications [8] - including quantum computing. Harneit [9] proposed trapping an atom inside a fullerene cage and using the electron spin of the trapped atom as a qubit. Harneit's scheme has a number of advantages over other types of NMR-based proposals: the fullerene cage protects the qubit from chemical interactions and slows decoherence processes, and the carbon shell is large enough that the sphere may be physically manipulated in a large-scale system.

A viable quantum computing strategy must fulfil several requirements [7]:

- *The qubits must be well-characterized.* In Harneit's scheme, binary 1 and 0 states are identified with the spin up and spin down states of the electrons in the incarcerated atom. Nuclear spins may also be used as qubits [17].

- *It must be possible to initialize the qubits in a known initial state.* As in other NMR based systems, the spins are initialized through alignment with an external magnetic field.

- *The qubits must exhibit decoherence times which are much longer than the time required for gate operations.* Electrons on incarcerated atoms in

fullerene cages are known to have relatively long decoherence times [1] [9] [19]. The electron spin of the trapped atom may also be coupled to the nuclear spin using a radio frequency field; in this scenario, the nuclear spin acts a qubit while the electron spin is coupled and decoupled from the nuclear spin in order to flip the nuclear spin state [17]. Without the application of an RF field, the nuclear spin is otherwise weakly coupled to the surrounding spins, making the nuclear spin ideal as a qubit. In addition, the coupling between the electron and nuclear spins may be exploited to apply phase operations to the nuclear spin much more rapidly than in conventional NMR [17].

- *The qubits must interact under a universal set of quantum gates.* Fullerene qubits are coupled to one another by the magnetic dipole interactions of neighbouring qubit spins. The spins may be manipulated by tuning microwave pulses to the resonant frequency of each particular bit [9].

- *It must be possible to measure the state of a specific qubit.* There are several proposals for measuring the state of particular spins including, conventional Electron Paramagnetic Resonance (EPR), micro-SQUIDS or Optically Detected Magnetic Resonance [17].

The Quantum Zeno effect, in which rapid measurement continuously forces a bit into a known state, might also be exploited to prevent decoherence. Related techniques - *bang bang* methods [23] - employ rapid bit flips to deter phase evolution. Morton [17] has also suggested using phase shifts to prevent amplitude evolution. However, *bang bang* strategies may only be implemented successfully in cases where the decay time far exceeds the gap between the application of pulses [23]. An understanding of relaxation and decoherence processes in the electronic and nuclear spins of the incarcerated atom is therefore neccessary to the design of a quantum computer.

The relaxation of an electron spin qubit in a fullerene cage may be probed by studying a simple spin model of the electron-fullerene system. The tiniest fullerenes, C_{20} - C_{30}, contain a sufficiently small number of lattice sites that

the system may be treated numerically using the Heisenberg model. Since each site is occupied by one spin up electron or one spin down electron, the dimension of the Hamiltonian for a system with N sites is 2^N. The number of sites which can be studied numerically is limited by computational storage: current studies in fullerenes have successfully treated up to 30 sites [11].

In this thesis, I use a Lanczos algorithm to compute the low energy states of an endohedrally doped C_{20} fullerene molecule described by the Heisenberg model. The dependence of the spin relaxation behaviour on the external fields and the coupling between the fullerene and the dopant is investigated as a function of time.

Treating the fullerene in the Heisenberg model presents a significant simplification of the real molecule, discarding all electron conduction effects; however, because it is often very difficult to exactly solve quantum many-body systems, employing computational methods and toy models may yield physical insights into the relaxation of a qubit coupled to a mesoscopic bath.

1.2 Properties of endohedral fullerenes

Endohedral fullerenes, in which a dopant atom is trapped within the carbon cage, first occured incidentally during the production of regular fullerenes [4]. Modifying the ambient gas or doping the carbon source allows finer control over the incarcerated atom. Macroscopic quantities of a particular doped fullerene can be obtained using High Performance Liquid Chromatography to separate different allotropes and different dopants [4].

In a fullerene molecule each carbon atom is bound to three others, forming a polyhedron with twelve pentagonal faces. Additional hexagonal faces are added as the number of carbons increases - cages containing more than one hundred atoms have been observed [6]. Many techniques have been developed to synthesize fullerene compounds; most methods are based on laser evaporation or arc discharge between graphite rods [4].

In the quantum-computing scheme proposed by Harneit [9], a Group V

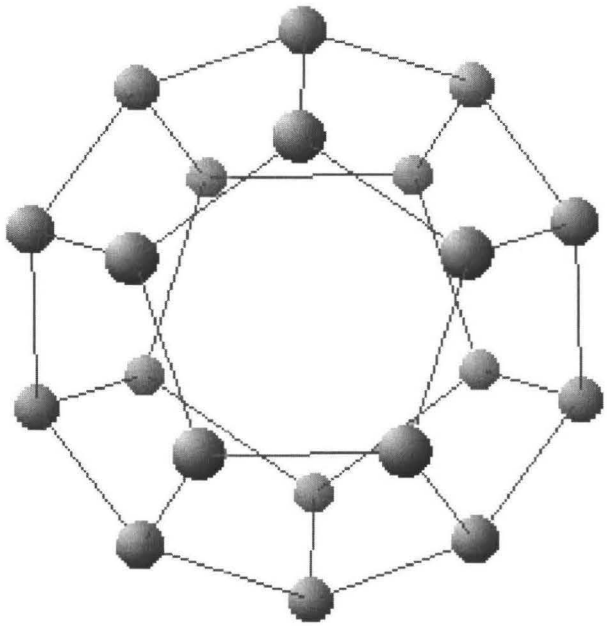

Figure 1.1: C_{20}, the smallest fullerene, contains 20 carbon atoms arranged in a structure with 12 pentagonal faces.

atom - such as nitrogen - is trapped inside a fullerene cage and the qubit state is encoded in the electron spin of the dopant. Unlike other elements, Group V atoms do not transfer charge to the carbon shell and so the trapped atoms interact very weakly with the fullerene. The magnitude of the interaction between the fullerene and the dopant can be estimated with respect to the magnitude of the interactions between each of the carbon atoms by examining the orbital overlap. Density-functional calculations on endohedral nitrogen implanted in C_{60} indicate that there is a 2% overlap between the nitrogen and carbon orbitals [15]. This implies that the coupling between the dopant and the fullerene electrons is weaker than the coupling between electrons on adjacent carbons atoms.

C_{20} (Figure 1.1) is the smallest of the fullerene cages; this compound was recently synthesized by Prinzbach and colleagues [20]. Due to the increased curvature of the cage and the higher strain in the π-bonds on the pentagonal faces, C_{20} is not as stable as larger fullerenes. Although forming a qubit

from C_{20} is impractical, the smallest fullerene has many features in common with larger cages. Like C_{60}, the lattice sites of C_{20} are all identical and this symmetry, along with the small number of lattice sites, makes C_{20} a fruitful system to describe exactly using simple spin models.

1.3 Experimental Work

Electron Paramagnetic Resonance (EPR) experiments have been conducted on bulk quantities of nitrogen-doped C_{60} dissolved in CS_2 [18]. EPR techniques exploit the unpaired electrons in the nitrogen p-orbitals - these spins align along the $\hat{z}$ axis in the direction of an external magnetic field.

The T_1 relaxation time describes how quickly a spin aligned antiparallel to a magnetic field releases energy to the environment and relaxes back to a state parallel to the external field. This process is investigated by applying a radiofrequency pulse of the appropriate duration and frequency to rotate the p-electron spins antiparallel to the field. If a second magnetic field, B_x, oscillates in the $\hat{x}$ direction, the electron spins will precess and induce a current in an external pick-up coil which is proportional to the magnitude of the magnetization in the $\hat{z}$ direction,

$$M_z(t) = M_0(1 - 2e^{-t/T_1}). \tag{1.1}$$

The T_2 decoherence time describes how an ensemble of spins in a magnetic field, B_z lose phase coherence. If B_z is slightly inhomogenous, the Zeeman splittings in the nitrogen p-electrons will vary and the spins will have slightly different resonant frequencies. If a microwave pulse is applied which rotates the p-electron spins into the $x - y$ plane then some spins will precess more rapidly than others because of small difference between the resonances. The magnetization in the $X - Y$ plane decays according to

$$M_{xy}(t) = M_0(1 - 2e^{-t/T_2}). \tag{1.2}$$

Morton [17] has shown that the relaxation and decoherence times are decreased by magnetic inhomogeneities introduced by the presence of nuclear magnetic in the solvent. He has also demonstrated that trapping the dopant inside the fullerene cage increases the relaxation and decoherence times substantially - T_1 is as high as 0.25 ms in some solvents.

The T_1 relaxation and T_2 decoherence processes limit the time over which a spin is valid as a qubit. If the coupling between the qubit and the fullerene is strong enough, the qubit may relax by emitting energy into the carbon cage, decreasing the relaxation time of the qubit. It is therefore pertinent to examine $\langle \sigma_z(t) \rangle$ to determine how the signal may be corrupted by interaction with the fullerene.

Chapter 2

Theory

2.1 Hamiltonian for a qubit-fullerene system

In the environment of an ideal qubit external magnetic fields and temperature are controlled so that only one energy level is accessible to the dopant. Because the spin is unable to relax by releasing energy into the fullerene or the environment, the T_1 time is infinite. However, in real systems the separation between levels is small enough that the dopant may exchange energy with the fullerene - and the environment. Consequently, it is pertinent to examine the T_1 relaxation process in a model system over a small number of energy levels that are made accessible when the qubit spin is placed in an initial state which is a linear combination of a few low-lying levels.

In the Hubbard model, each atom contains a single π-electron orbital which may be occupied by up to two electrons with anti-parallel spins. Electrons can hop between nearest-neighbour sites $\langle i, j \rangle$ with a tunneling probability, t_{ij}. The Coloumb repulsion between two electrons on the same lattice site increases the energy of the system by U when two electrons occupy the same site. The Hamiltonian reads:

$$\hat{H} = \sum_{<i,j>} t_{ij} \hat{c^{\dagger}_{i\uparrow}} \hat{c}_{j\uparrow} + U \hat{n}_{i\uparrow} \hat{n}_{j\downarrow}. \tag{2.1}$$

In the large U limit at half-filling, the on-site Coulomb interaction discourages doubly-occupied sites and the Hubbard Hamiltonian reduces to the Heisenberg Hamiltonian:

$$\hat{H} = \sum_{<i,j>} J_{ij} \vec{S}_i \cdot \vec{S}_j \tag{2.2}$$

The spin operators, $\vec{S}$, can be written in terms of the electron creation and annihilation operators, c and $c^\dagger$; the exchange energy, J_{ij}, is t_{ij}^2/U [2]. In order to model the relaxation processes of the dopant electron spin, it is sufficient to treat the fullerene using the Heisenberg model - nitrogen and phosphorous atoms implanted in C_{60} do not donate electrons to the carbon cage, so conduction effects in the fullerene may be ignored.

Values of U and t_{ij} for C_{20} may be estimated from parameters calculated for C_{60} and C_{70} under the an extended Hubbard model - the SSH Hamiltonian. In this description, values for t_{ij} are refined by expanding the coupling to first order in bond length. The most significant contribution to the hopping part of this Hamiltonian is due to the following term:

$$\hat{H} = \sum_{<i,j>} \left(t_0 - \alpha(l_{ij} - l_0)\right) c_{i\uparrow}^\dagger c_{j\uparrow} + U n_{i\uparrow} n_{j\downarrow}. \tag{2.3}$$

Yu [24] has made estimates of t_0 and α by adjusting the parameters to produce gaps between the highest occupied molecular orbital (HOMO) and the lowest unoccupied molecular orbital (LUMO) states which are consisent with a pseudopotential density function approach. From local density approximation methods (LDA), $t_0 = 2.72$ eV in C_{60}, along the $1.46\mathring{A}$ pentagon-hexagon bond. $\alpha = 5.6$ eV/$\mathring{A}$ so, $t = 2.72 - 5.6 \times (1.40 - 1.46\mathring{A}) = 3.0$ eV along the $1.40\mathring{A}$ hexagon-hexagon bond.

Estimates for U have been obtained by identifying low energy states as a function of U/t in the Hubbard model - U lies in the range $2t_{ij} \leq U \leq 5t_{ij}$ [14]. The coupling along the carbon-carbon bonds in a fullerene is $0.54 \leq J = t^2/U \leq 1.4$ eV.

Implanting a dopant spin at the centre of the fullerene requires an additional interaction term:

$$\eta \sum_i \vec{\sigma} \cdot \vec{S}_i. \tag{2.4}$$

Since all the C_{20} lattice sites, (i) are equivalent, the exchange interaction between each carbon atom and the dopant is given by a constant, η.

For nitrogen-doped cages, the pertinent exchange interaction occurs between the p-orbitals of the nitrogen and carbon atoms. The 3p electrons in the nitrogen couple to $S = 3/2$ states by Hund's rule: the interaction between the fullerene and the qubit will be antiferromagnetic and, hence, η is positive.

2.2 EPR in a qubit-fullerene system

The qubit state is encoded in the fullerene-dopant system using the σ_z component of the dopant spin. External magnetic fields may be manipulated to write - and read - the qubit state using Electron Paramagnetic Resonance (EPR). As in other NMR-based quantum computer schemes, a large static magnetic field (B_z) is used to define a preferred direction, while a second field (B_x) oscillates perpendicular to the first. Electromagnetic pulses of appropriate duration and frequency can be used to flip the spins between the spin up and spin down states. The spins precess in the B_x field and - in bulk systems - σ_z may be measured by observing the current that this magnetic moment induces in an external coil.

First, consider the Hamiltonian for a single qubit:

$$\hat{H}_q = g\mu_B B_z \hat{\sigma}_z + \gamma_e B_x \cos(\omega t + \phi)\hat{\sigma}_x. \tag{2.5}$$

This describes a fullerene implanted with a spin 1/2 dopant, denoted by $\hat{\sigma}$. By setting $\omega_e = g\mu_B B_z$ and $\Delta = B_x\gamma_e/2$, the Hamiltonian may be written

in the basis of σ_z:

$$\hat{H}_q = \begin{pmatrix} \frac{\omega_e}{2} & \Delta\cos(\omega t) \\ \Delta\cos(\omega t) & -\frac{\omega_e}{2} \end{pmatrix} \tag{2.6}$$

Choosing a reference frame which revolves at the frequency of the applied microwave field allows the explicit time dependence of the Hamiltonian to be eliminated. A change of basis into this frame is accomplished by the rotation operator, $\hat{U}$:

$$\hat{U} = \begin{pmatrix} e^{i\omega t/2} & 0 \\ 0 & e^{-i\omega t/2} \end{pmatrix} = e^{i\hat{\sigma}_z\omega t}. \tag{2.7}$$

Now $|\psi_{rot}\rangle = \hat{U}|\psi\rangle$, so the time-dependent Schrodinger equation is

$$\hat{H}_q\hat{U}^\dagger|\psi_{rot}\rangle = i\frac{\delta}{\delta t}(\hat{U}^\dagger|\psi_{rot}\rangle) = \sigma_z\omega\hat{U}^\dagger|\psi_{rot}\rangle + \hat{U}^\dagger(i\frac{\delta}{\delta t}|\psi_{rot}\rangle). \tag{2.8}$$

Applying $\hat{U}$ to this equation yields an effective Hamiltonian for ψ_{rot}:

$$\hat{H}_{eff}|\psi_{rot}\rangle = i\frac{\delta}{\delta t}|\psi_{rot}\rangle = (\hat{H}_q - \sigma_z\omega)|\psi_{rot}\rangle \tag{2.9}$$

In the "rotating wave approximation" the fast oscillating terms, $e^{2i\omega t}$ and $e^{-2i\omega t}$ can be discarded. The effective Hamiltonian, $\hat{H}_{eff}$ in matrix form

$$\hat{H}_{eff} = \begin{pmatrix} \frac{1}{2}(\omega_e - \omega) & \Delta e^{i\omega t}\cos(\omega t) \\ \Delta e^{-i\omega t}\cos(\omega t) & \frac{1}{2}(\omega_e - \omega) \end{pmatrix} \approx \begin{pmatrix} \frac{1}{2}(\omega_e - \omega) & \Delta \\ \Delta & \frac{1}{2}(\omega_e - \omega) \end{pmatrix} \tag{2.10}$$

The freqency of the oscillating B_x field may be tuned to resonate with the Zeeman splitting induced by the static field, B_z. Since the electrons on the fullerene will have different resonances than the qubit, the Hamiltonian may be simplified by applying magnetic fields only to the incarcerated spin. This is realistic for the case where the qubit is a muon - the muon magnetic moment is $4.4904514 \times 10^{-26}$ J T^{-1} while the electron magnetic moment is $9.2847701 \times 10^{-24}$ J T^{-1}. At resonance, the B_z field on the fullerene is effectively turned

off ($\omega_e - \omega = 0$), while the qubit continues to precess in the applied fields. In the full Hamiltonian the spin of the dopant is denoted by σ while S_i are spins on the fullerene and $< i, j >$ denotes nearest-neighbour sites:

$$\hat{H} = \varepsilon\hat{\sigma}_z + \Delta\hat{\sigma}_x + \sum_{\langle i,j\rangle} J_{ij}\vec{S}_i \cdot \vec{S}_j + \eta \sum_i \vec{\sigma} \cdot \vec{S}_i. \tag{2.11}$$

The difference between the resonant frequency of the electrons and the driving frequency of the B_x field, $\frac{1}{2}(\omega_e - \omega)$, may be written as ε. At $t = 0$, the system is initialized in the low energy state with the dopant spin down - denoted $\phi_{\downarrow 0}$. The eigenvector for this state is determined by solving for the ground state of the Hamiltonian,

$$\hat{H} = \varepsilon\hat{\sigma}_z + \sum_{<i,j>} J_{ij}\vec{S}_i \cdot \vec{S}_j + \eta \sum_i \vec{S}_i \cdot \vec{\sigma}. \tag{2.12}$$

The eigenstates of the full Hamiltonian (Equation 2.11) are denoted ψ_k. The evolution of the ground state, $|\Psi(0)\rangle = |\phi_{\downarrow 0}\rangle$, is described by

$$|\Psi(t)\rangle = e^{i\hat{H}t}|\Psi(0)\rangle = e^{i\hat{H}t}\sum_k a_{0,k}|\psi_k\rangle = \sum_k a_{0,k}e^{iE_k t}|\psi_k\rangle. \tag{2.13}$$

where the coefficients $a_{0,k} = \langle\psi_k|\phi_{\downarrow,0}\rangle$ describe the overlap between the initial state, $\phi_{\downarrow,0}$, and the eigenstates of the full Hamiltonian.

Applying an oscillating B_x field mixes some of the low-lying states and the spin of the dopant, $\langle\sigma_z(t)\rangle$, will evolve according to

$$\langle\Psi(t)|\sigma_z|\Psi(t)\rangle = \sum_k (\frac{a_{0,k}^2}{2}\langle\psi_k|\sigma_z|\psi_k\rangle + \sum_{j>k} a_{0,k}a_{0,j}cos((E_j - E_k)t)\langle\psi_k|\sigma_z|\psi_j\rangle). \tag{2.14}$$

Provided the coupling, η between the dopant and the fullerene cage is small, only the low-lying states will mix and the time evolution of the system can be determined exactly.

2.3 Variations on the Hamiltonian

It is also useful to consider the case where the external fields act on the fullerene as well as on the dopant:

$$\begin{aligned}\hat{H} =& gB_z(\mu_B \sum_i \hat{S}_{iz} + \mu_Q \hat{\sigma}_z) + gB_x \cos(\omega t + \phi)(\mu_Q \hat{\sigma}_x + \mu_B \sum_i \hat{S}_{ix}) \\ &+ \sum_{<i,j>} J_{ij} \vec{S}_i \cdot \vec{S}_j + \eta \sum_i \vec{\sigma} \cdot \vec{S}_i.\end{aligned} \tag{2.15}$$

The system is first aligned in the ground state in the presence of a static B_z field. When a microwave field, B_x, is applied at resonance B_z is cancelled on all the spins in the system. If the qubit has a magnetic moment (μ_Q) that differs from the electron moments in the fullerene (μ_B), the Hamiltonian no longer commutes with S^2 and the total S_z of the system may evolve non-trivially.

2.4 Computational considerations

The amount of memory required to store the Hamiltonian and the time required to carry out diagonalization routines limit the size of the lattice that may be studied. For the Hubbard model, up to two electrons may occupy each lattice point, so there are four possible states for each site: $\{0,0\}$, $\{\uparrow,\downarrow\}$, $\{\downarrow,0\}$, $\{\uparrow,0\}$. For the Heisenberg model each lattice site possesses one electron, so the possible states are $\{\downarrow\}, \{\uparrow\}$. Because the Hilbert space for the Hubbard model on a lattice with N sites has a dimension 4^N while the number of possible states for the Heisenberg model is 2^N, working with the Heisenberg model presents a substantial computational savings. In 16 bit precision a single eigenvector for a 28 site lattice in the full space of the Heisenberg Hamiltonian requires $\frac{16\times 2^{28} bits}{8\times(1024)(1024)(1024) bits/GB} \approx 0.5$ GB of memory.

Although it is impractical to fully diagonalize problems involving more than a dozen lattice sites, numerical methods exist which allow for the exact solution of a small number of extremal states. In addition, the Hilbert space

may be reduced by invoking commutation relations to block-diagonalize the Hamiltonian. For example, the Heisenberg Hamiltonian commutes with S^2, S_z and spatial symmetry operations which are peculiar to each fullerene.

The Hamiltonian matrix is sparse - most of the elements are zero. The maximum number of non-zero elements is related to the connectivity: in the full Hilbert space of a lattice described by the Heisenberg model where each site has N_{nn} nearest neighbours, there are maximally $1 + N \times N_{nn}$ non-zero elements per row of the Hamiltonian. There is one diagonal term resulting from onsite interactions involving S_z and additional off-diagonal terms resulting from exchange of two electrons with opposite spins. The storage requirements can be further reduced by generating each row of the Hamiltonian twice - the first iteration determines the total number of non-zero elements and their indices, while the elements themselves are calculated in the second step.

For large systems, it is necessary to block diagonalize the Hamiltonian in order to reduce the number of non-zero elements that must be stored in memory. Reducing the size of the matrix also decreases the amount of time required for the Lanczos determination of the low-energy states. However, schemes for labelling the spin states become less efficient. In the full Hilbert space, each state is indexed by a binary number and the i^{th} digit corresponds to the ith lattice site - an $O(n)$ process. Block diaganalizing using the S^2 operator requires a more sophisticated labelling scheme, which is more time intensive.

The Lanczos routine has been developed to reliably compute extremal eigenvalues and eigenvectors for large, sparse matrices. The most intensive part of the algorithm is a matrix-vector multiplication, so the time required is quadratic in N for an $N \times N$ Hamiltonian. The technique generates an initial eigenvector in a subspace of the matrix and calculates subsequent states by generating orthogonal vectors [5]. For large systems, both PETSc (C) [3] and ARPACK (FORTRAN) [13] Lanczos routines produce equivalent results. PETSc includes routines for assembling matrices and vectors in parallel across several processors and the solution method - exact diagonalization, Lanczos

- can be selected at the command line without recompiling or modifying the code prior to running the executable.

2.4.1 Verifying numerical results

In order to test the validity of the low-energy spectra, smaller systems (C_{12}, rings) were solved using exact diagonalization methods (LAPACK). In addition, results for rings reproduce the Bethe ansatz [10]. For small systems SLEPc Lanczos routines do not return the correct degeneracies of the low-lying states; however, the low energy spectra are the same as those generated by LAPACK for large systems. In addition, the Lanczos routine may erroneously discard some states when multiple degeneracies occur. This problem comes about because of post-processing used to cull off spurious states. A state with $S = N$ should have a degeneracy that is $2N + 1$-fold; this information can help to identify the incorrect degeneracies in systems which are too large to diagonalize exactly.

The validity of the eigenvectors produced using the Lanczos algorithm can be tested by taking the difference $||\hat{H}\psi - E\psi||$. When this value is close to 0 the eigenvalues and eigenvectors converge upon the exact values.

The evolution of the dopant spin in time is characterized by the coefficients $a_{0,k} = \langle\psi_k|\phi_{\downarrow 0}\rangle$, where $\phi_{\downarrow 0}$ is the ground state eigenvector of the system without a B_x field acting on the dopant. Applying this field constitutes a change of basis: the coefficients $a_{0,k}$ describe how to transform from the old ground state to the new eigenstates of the full Hamiltonian with the B_x field. The initial state, $\Psi(0)$ can be written in the new basis of the full Hamiltonian if enough of the higher-energy states are calculated. The first k_{max} eigenvectors of the full Hamiltonian, ψ_k, provide an accurate representation of $\Psi(0)$ if

$$A = \sqrt{1 - \sum_{k=1}^{k_{max}} a_{0,k}^2} \to 0. \tag{2.16}$$

A is the maximum contribution to the amplitude from the missing states. If

the sum over $a_{0,k}^2$ is only slightly less than 1 the missing states have a relatively small amplitude compared to the states that are included and the behaviour of $\langle \sigma_z(t) \rangle$ is not substantially affected.

Chapter 3

Results

The low-energy states of the fullerene systems described by the Heisenberg model were calculated using both PETSc (C) and ARPACK (Fortran) Lanczos routines. For all cases the J coupling between sites was set to 1; these results (Appendix A) reproduce Konstantinidis's values for the energies of the low-lying states [11]. The ground states all have the property $S_z = 0$ as expected for a Heisenberg antiferromagnet with an even number of sites [16] and all have $S^2 = 0$.

However, the degeneracies of some of the states evaluated using the Lanczos method are incorrect as discussed in section 2.4.1. This problem is observed in C_{12} where the expected degeneracy of the $S = 1, S^2 = 2$ states should be a multiple of three. The Lanczos solution of C_{12} (Table 1) yields a nine-fold degeneracy for $E = -5.013103134044950$ - a multiplicity which is reproduced by the Lanczos routine (Table 2). However, the Lanczos algorithm reports a four-fold degeneracy for $E = -4.657885305020258$ (nine-fold degenerate in the exact solution) and a four-fold degeneracy for $E = -4.322917182968258$ (also nine-fold degenerate in the exact solution).

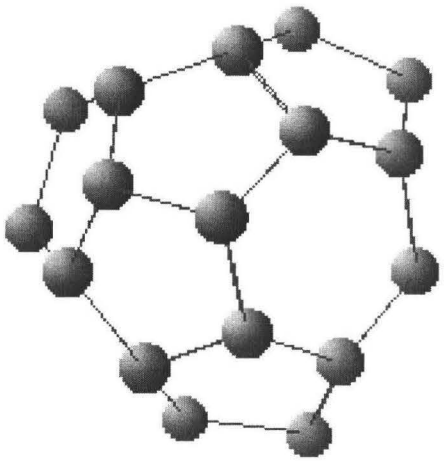

Figure 3.1: The td isomer of C_{28}. There are four hexagonal faces, none of which are directly adjacent. Eleven of the atoms in the background are obscured by atoms in the foreground.

3.1 Undoped fullerenes

There are two isomers of C_{28}; previous studies [11] examined only the "td" isomer (Figure 3.1). The "d2" isomer has a lower energy ground state than the "td" isomer (Table 6, Table 7), likely because there are two hexagon-hexagon edges in the "d2" isomer which help to reduce frustration (Fig 3.2).

Molecules of C_{12}, C_{20} and C_{60} all have the property that every atomic site is geometrically indistinguishable from the other sites on the lattice. Given that C_{12} and C_{20} have first excited states that are highly degenerate, it may be expected that the first excited state of C_{60} might also be highly degenerate in the Heisenberg model.

The low-energy spectra of C_{20} is shown (Table 3). The gaps between adjacent energy levels are sufficiently large that thermal excitations are negligible. A gap of $9.72-9.40 = 0.32$ eV is equivalent to 3500 K, so this excitation cannot be obtained thermally. The energy differences between the ground state and the first excited state of the larger fullerenes (Tables 4,5,6,7) are smaller, but these energies still correspond to large temperatures. It is therefore sufficient to treat the system in the low-temperature limit.

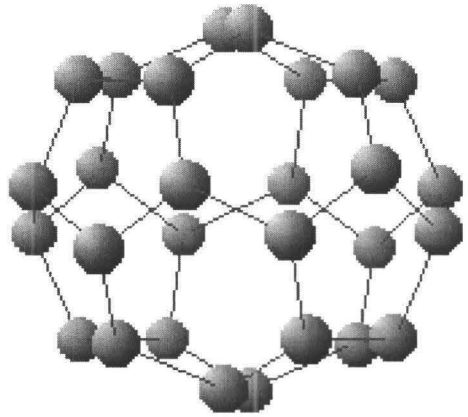

Figure 3.2: The d2 isomer of C_{28}. There are four hexagonal faces, each of which is directly adjacent to one of the other hexagonal faces.

3.2 Endohedral doped fullerenes

The Hamiltonian describing the scenario in which the external field acts only on the qubit is considered first (Eq. 2.11). It is assumed that there are no effective external fields on the fullerene spins, so B_x and B_z act only on the qubit. The effect of modifying the external fields and the η coupling between the fullerene and the qubit is probed by examining $\langle \sigma_z \rangle$ as a function of time. In the presence of the B_x field, the ground state mixes with one or more higher-energy states and the spin undergoes Rabi oscillations.

In general, when $\eta = 0$, the fullerene and qubit are completely decoupled and the frequency of the qubit oscillations is $\sqrt{B_x^2 + B_z^2}$. In this state, the total spin of the fullerene is $S_{fullerene} = \sum_i S_i = 0$. When η is increased by a small amout, the total spin of the fullerene remains 0 and the ground state eigenvector is unchanged. For all the systems of fullerene-type symmetry which have been studied under the Heisenberg model (C_{20} - C_{28}), the ground state is a singlet and $S_{fullerene} = 0$. Thus, in the ground state, $\eta \sum_i \vec{S}_i \cdot \vec{\sigma} = \eta(\sigma \cdot S_{fullerene}) = 0$, and the coupling between the qubit and the fullerene does not perturb the lowest energy state.

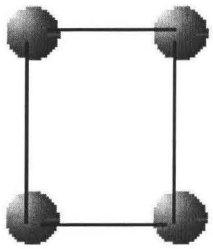

Figure 3.3: 4-site ring. The qubit is coupled to each site antiferromagnetically.

3.2.1 4-site, 10-site rings, triangular pyramid

It is instructive to first examine small systems to identify significant behaviours. For lattices with fewer than 10 sites the Hamiltonian may be fully diagonalized using the ARPACK option in the PETSc library: $\sum_k a_{0,k}^2 = 1$ to the precision of the calculated eigenvectors (ie, $\sum_k a_{0,k}^2 < 10^{-16}$) for this method as all the possible states are determined (Eq. 2.14).

For rings with 4 or 10 sites (Fig. 3.2.1) the ground state is a non-degenerate singlet. When a qubit is uncoupled or weakly coupled to the ring the bit precesses with a frequency equal to $\sqrt{\Delta^2 + \varepsilon^2}$ (Eq. 2.11) - this is simply the precession frequency of a bare qubit in the magnetic fields B_z and B_x. For small values of η the ground state of the fullerene is unperturbed by the addition of the dopant and the total spin of the system is $S = 1/2$ (Table 10).

When the coupling is increased past some critical amount ($\eta \approx 1.05$ for the four-site ring with $B_z = B_x = 0.1$) the ground state is perturbed. There are critical values of η where the ground state of the fullerene changes from $S = 0$ to $S = 1, 2, 3...$ (Tables 12, 11).

In Figure 3.4 the red line depicts the Rabi oscillations of the qubit below the critical value of η. In this case, η is small enough that the qubit state does not influence the electronic structure of the fullerene.

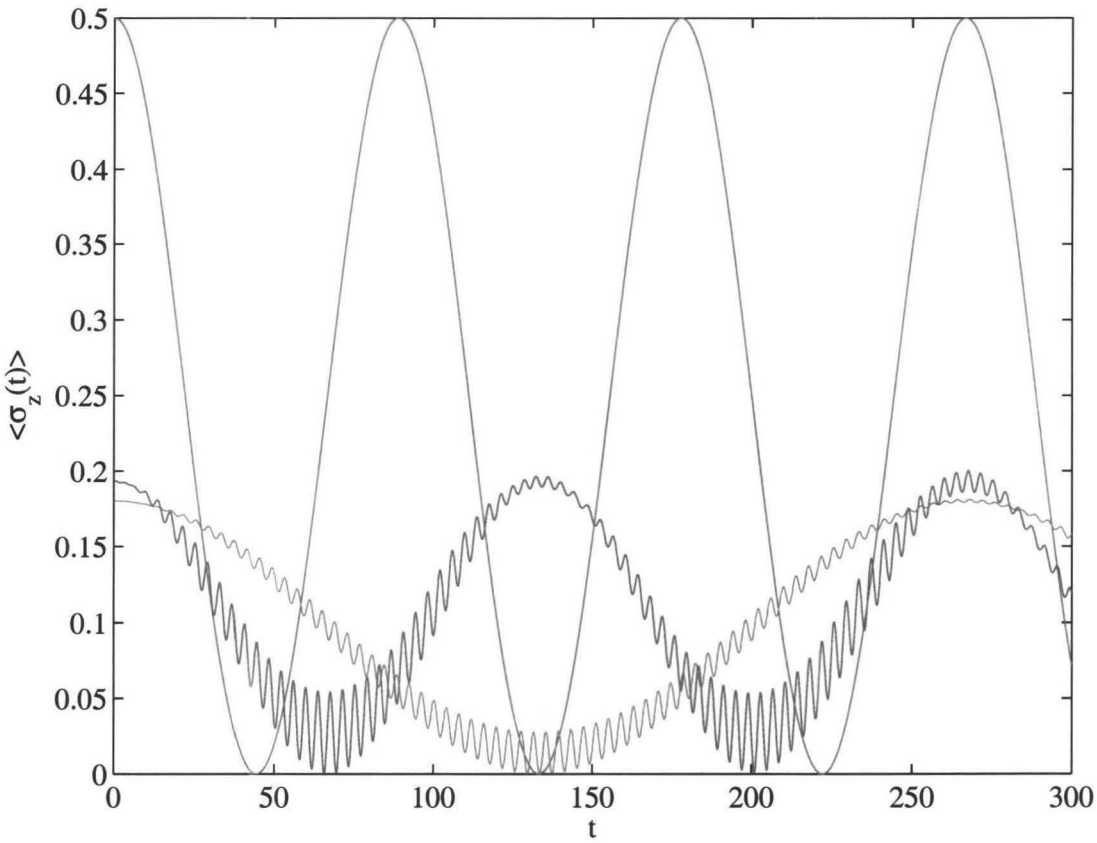

Figure 3.4: Oscillations on a 4-site ring with different η couplings between the fullerene and dopant. LAPACK has been used to diagonalize the full Hamiltonian. **red:** $\eta = 0.1$, $B_z = 0.1$, $B_x = 0.1$, **green:** $\eta = 0.5$, $B_z = 0.1$, $B_x = 0.1$, , **blue:** $\eta = 0.5$, $B_z = 0.2$, $B_x = 0.2$.

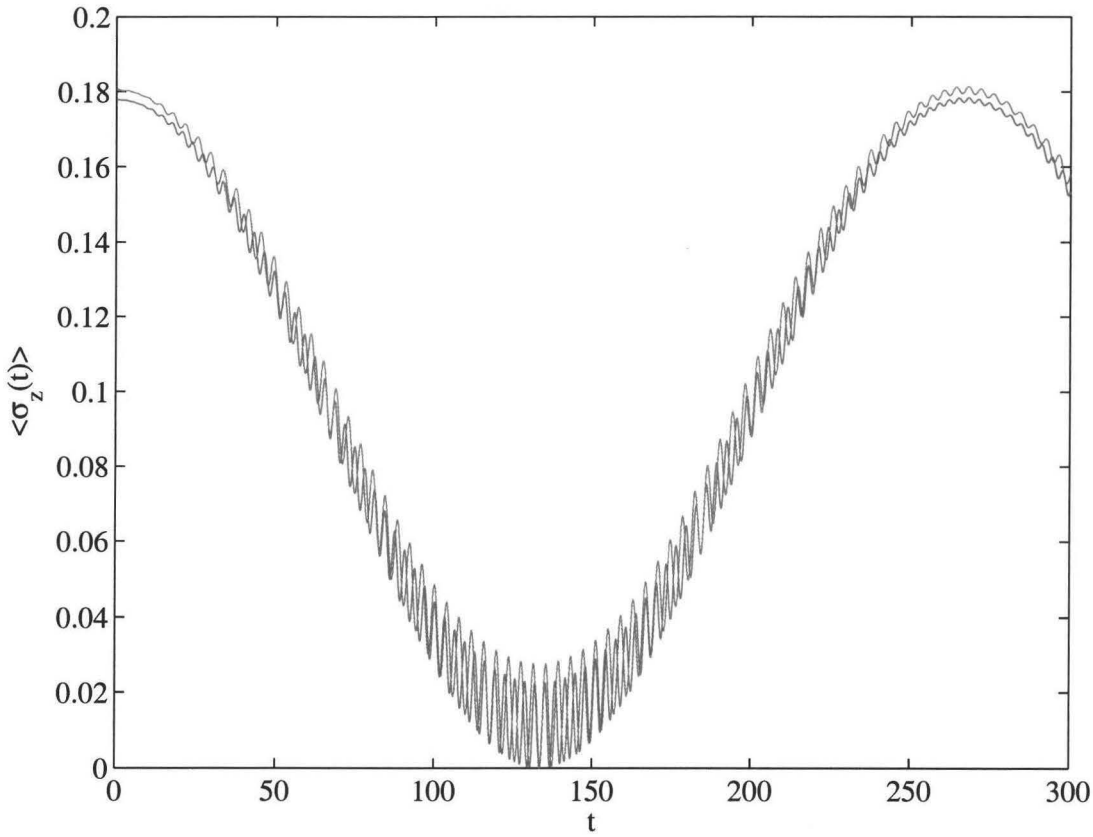

Figure 3.5: Oscillations of $\langle \sigma_z(t) \rangle$ on a 4-site ring with different η couplings between the ring and dopant. LAPACK has been used to diagonalize the full Hamiltonian **red:** $\eta = 1.3$, $B_z = 0.1$, $B_x = 0.1$, , **green:** $\eta = 1.05$, $B_z = 0.1$, $B_x = 0.1$, .

When coupling between the qubit and the cage is increased past the critical level, the spin of the fullerene is no longer 0 and the qubit spin may relax by releasing energy into the fullerene. When η is larger than the critical value and external fields are applied to the qubit, states with different values of S^2 are mixed and S^2 is no longer a good quantum number (Tables 8,9). Since the coupling mixes states with different total spin, applying the B_x field gives access to several levels with distinct energies. The admixture of these levels leads to high-frequency oscillations in $\langle \sigma_z(t) \rangle$. The gaps between levels accessed when the B_x field is applied scale linearly with $\sqrt{B_z^2 + B_x^2}$.

As the number of lattice sites on a ring increases, the first critical value of η (for the transition from an $S = 0$ fullerene to an $S = 1$ fullerene decreases (Figure 3.6). The frequency of the highest amplitude oscillation again depends on the gap between the lowest-energy dopant spin-down state and the lowest energy dopant spin-up state; the size of this gap continues to increase linearly with $\sqrt{B_z^2 + B_x^2}$. The frequency of this oscillation is the same for both rings of ten site and rings of four sites, in the regimes where the respective spins of the rings are the same (ie, $S_{fullerene} = 1$ for $\eta = 1.05$ for the 10-site and 4-site rings - Figs. 3.6, 3.5.)

While the frequency of the highest-amplitude oscillation is unchanged when the total spin of the fullerene is unmodified by the coupling between the ring and the qubit, increasing the coupling strength between the dopant and the ring reduces the amplitude of the higher frequency oscillations. In addition, introducing more sites into the lattice decreases the critical value of η for which the coupling and external fields mix states with different total spins - the first critical value of η on the 4-site ring is ≈ 1.05 while the first critical value of η on the 10-site ring is ≈ 0.5.

The evolution of $\langle \sigma_z \rangle$ for a doped triangular pyramid is also considered. This is the smallest three dimensional structure, but it is dissimilar from the majority of the small fullerenes in that the ground state is doubly degenerate. However, the splittings between energy levels induced by the external fields are the same as for the ring with four sites and the same value of η in the regime

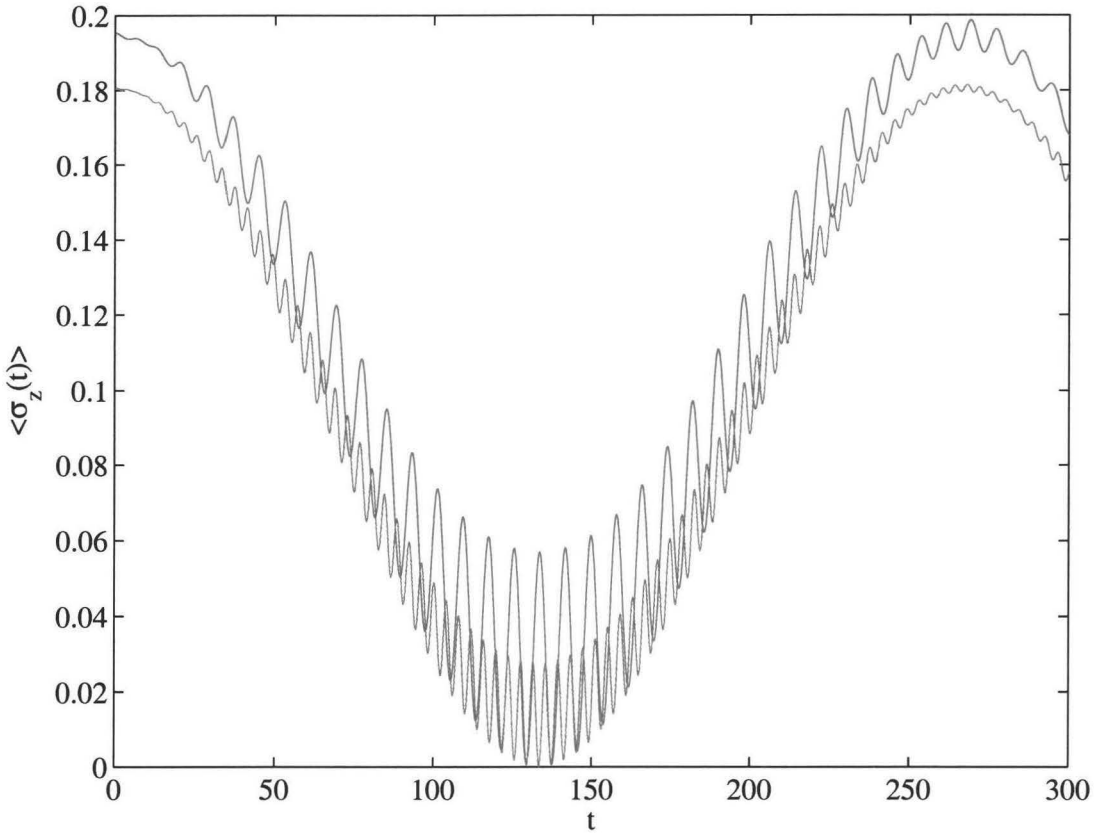

Figure 3.6: Oscillations of $\langle \sigma_z(t) \rangle$ on a ring with 10 sites with different η couplings between the ring and dopant. The Lanczos algorithm has been used to determine the lowest n_{evr} eigenvectors. **red:** $\eta = 0.5$, $B_z = 0.1$, $B_x = 0.1$, $n_{evr} = 50$, $A = 7.300048 \times 10^{-8}$, **green:** $\eta = 1.05$, $B_z = 0.1$, $B_x = 0.1$, $n_{evr} = 120$, $A = 6.580175 \times 10^{-8}$.

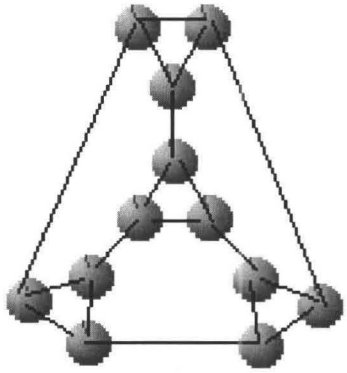

Figure 3.7: Topology of C_{12} (bond lengths are distorted).

where $S_{fullerene} = 1$. The evolution of $\langle \sigma_z(t) \rangle$ in time is therefore identical for the pyramid and the four-site ring.

3.2.2 C_{12} and C_{20}

C_{12} is the smallest lattice with fullerene-type structure: each of the sites has three nearest-neighbours and there are two different faces on the solid polyhedron - one which has an even number of sides and one which has an odd number of sides. In the fullerenes, each face is either a hexagon or a pentagon, while in C_{12} the faces are either triangular or hexagonal. The low-energy spectra of the undoped structure is similar to that of C_{20} (Fig 1.1) in that the ground state is a non-degenerate singlet while the first excited state is multiply degenerate (Table 1). Like C_{20} and C_{60}, all the lattice sites in C_{12} are geometrically indistinguishable.

On a single processor, exact diagonalization is time consuming for C_{12} and the Lanczos algorithm must be deployed to find the significant low-energy states which contribute to the initial state. The value of the parameter $A = \sqrt{1 - \sum_k a_{0,k}^2}$ (Eq. 2.16) is used as a test that the initial state can be described by a subset of the calculated eigenstates in the new basis when B_x is switched

Table 3.1: Test of basis completeness for C_{12}, $\eta = 1.05$,$B_z = 0.1$, $B_x = 0.1$

number of eigenvalues requested (n_{evr})	maximum amplitude of missing states $A = \sqrt{1 - \sum_k a_{0,k}^2}$
50	$1.4722470484351 \times 10^{-2}$
200	$1.4497693345365 \times 10^{-2}$
300	$1.1707424327781 \times 10^{-2}$
400	$6.322238007 \times 10^{-6}$

on. As the number of requested eigenvalues, n_{evr}, is increased it becomes more likely that higher energy states will be included (Table 3.1).

High-frequency oscillations are observed when 200 or more eigenvalues are requested for $\eta = 1.05$ and $B_z = B_x = 0.1$. If $\sum_k a_{0,k}^2$ is less than 10^{-4}, the oscillations still have similar behaviour to those that appear in the full solution as the missing states contribute many very small amplitude oscillations over a range of frequencies.

The ground state of C_{12} for $\eta = 1.3$, $B_z = 0.1$, $B_x = 0.0$ is threefold degenerate (Table 1). It does not matter which of these three states is selected as the initial state when the B_x field is turned on: when $\sqrt{1 - \sum_k a_{0,k}^2} \to 0$ the oscillations of $\langle \sigma_z(t) \rangle$ are identical for each of the three degenerate states.

If the coupling strength, η, is increased in the absence of external magnetic fields the qubit spin eventually forces the fullerene from the $S = 0$ state. As η is increased, the fullerene spins couple antiferromagnetically with the dopant and the total spin of the fullerene increases (Fig 3.2.2).

A qubit coupled to a 12-site ring perturbs the ground state of the system for $\eta > 0.4$ when $B_z = 0.1J$ and $B_x = 0.1J$ (Figure 3.2.2). The critical value of η for which the addition of the qubit perturbs the ground state of the 12-site ring is smaller than the critical value for the 10-site and 4-site rings - which is to be expected as the gaps between levels decrease as sites are added to the lattice.

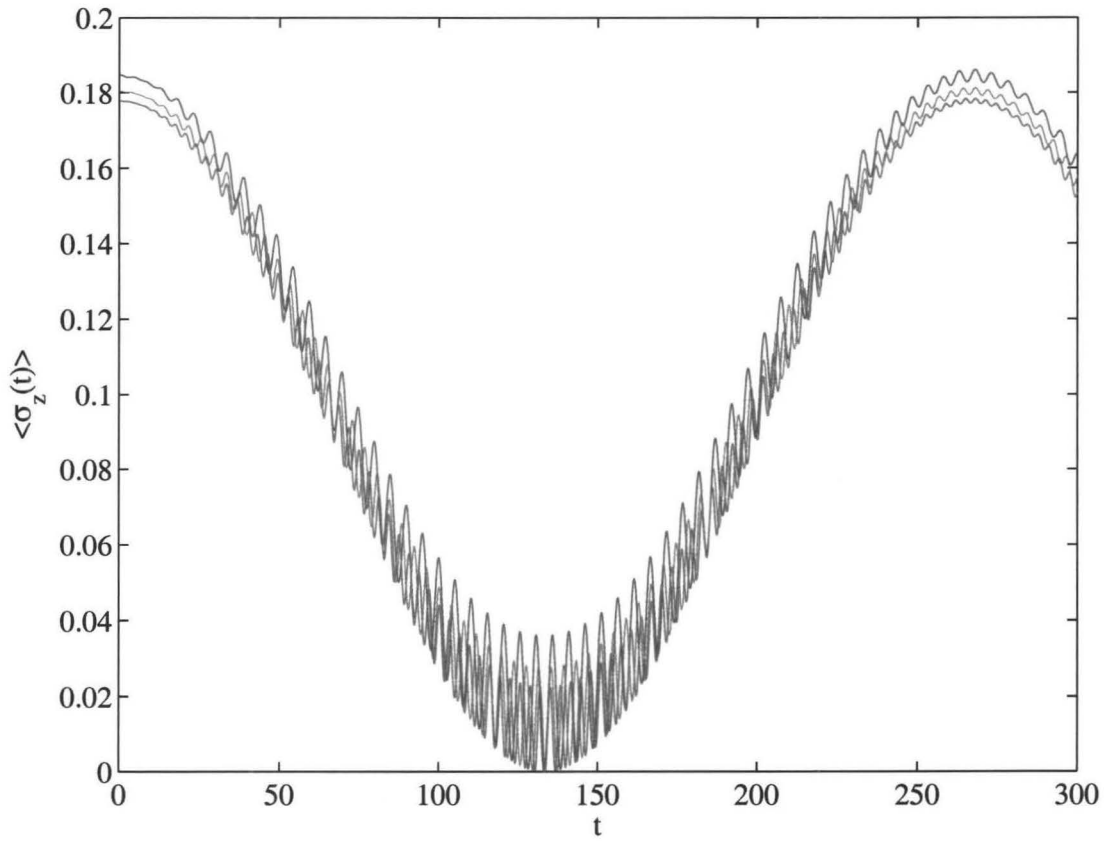

Figure 3.8: Oscillations of $\langle \sigma_z(t) \rangle$ on an endohedral doped C_{12} lattice.**red:** $\eta = 1.3$, $B_z = 0.1$, $B_x = 0.1$, $n_{evr} = 800$, $A = 2.068311 \times 10^{-6}$ **green:** $\eta = 1.05$, $B_z = 0.1$, $B_x = 0.1$,$n_{evr} = 400$, $A = 6.322238 \times 10^{-6}$ **blue:** $\eta = 0.8$, $B_z = 0.1$, $B_x = 0.1$. $n_{evr} = 200$, $A = 4.303477 \times 10^{-5}$

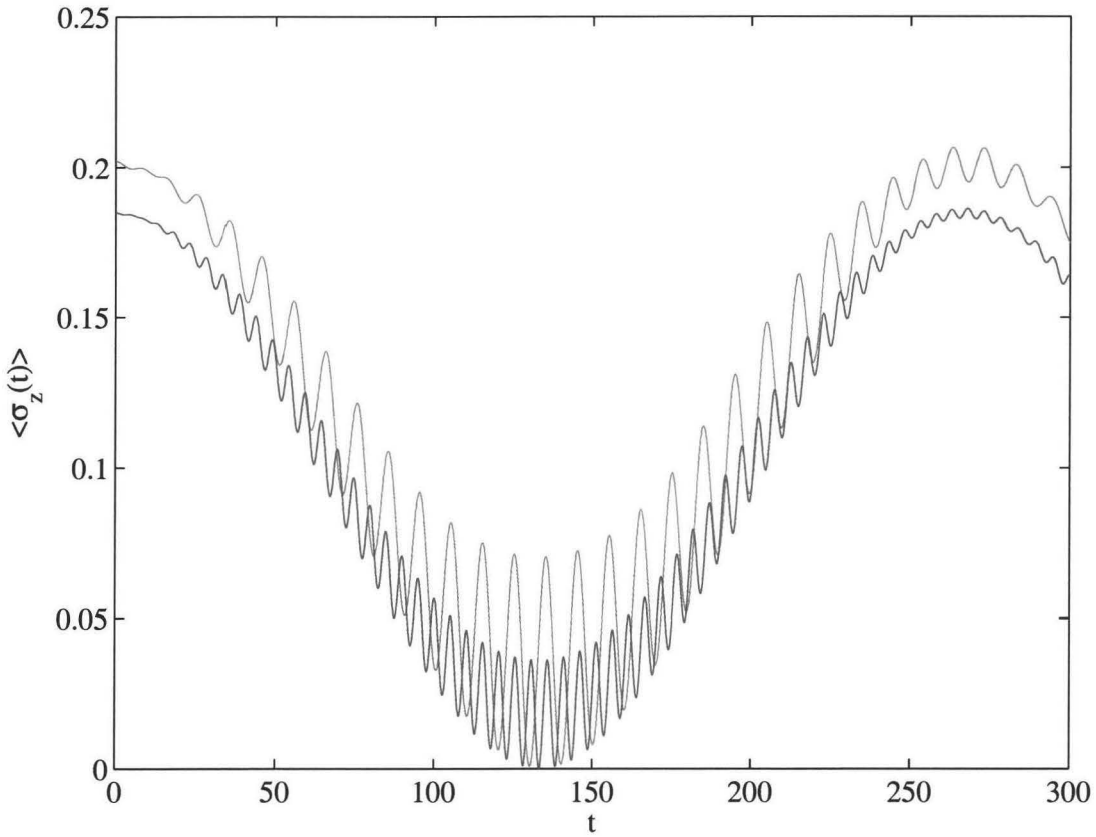

Figure 3.9: Oscillations of $\langle \sigma_z(t) \rangle$ on a centrally doped 12-site ring. **green: 12-site ring** $\eta = 0.4$, $B_z = 0.1$, $B_x = 0.1$, $n_{evr} = 100$, $A = 1.983003 \times 10^{-6}$ **blue: 12-site ring AND endohedral doped fullerene** $\eta = 0.8$, $B_z = 0.1$, $B_x = 0.1$. **Ring:** $n_{evr} = 100$, $A = 2.277003 \times 10^{-7}$. **$C_{12}$:** $n_{evr} = 200$, $A = 4.303477 \times 10^{-5}$.

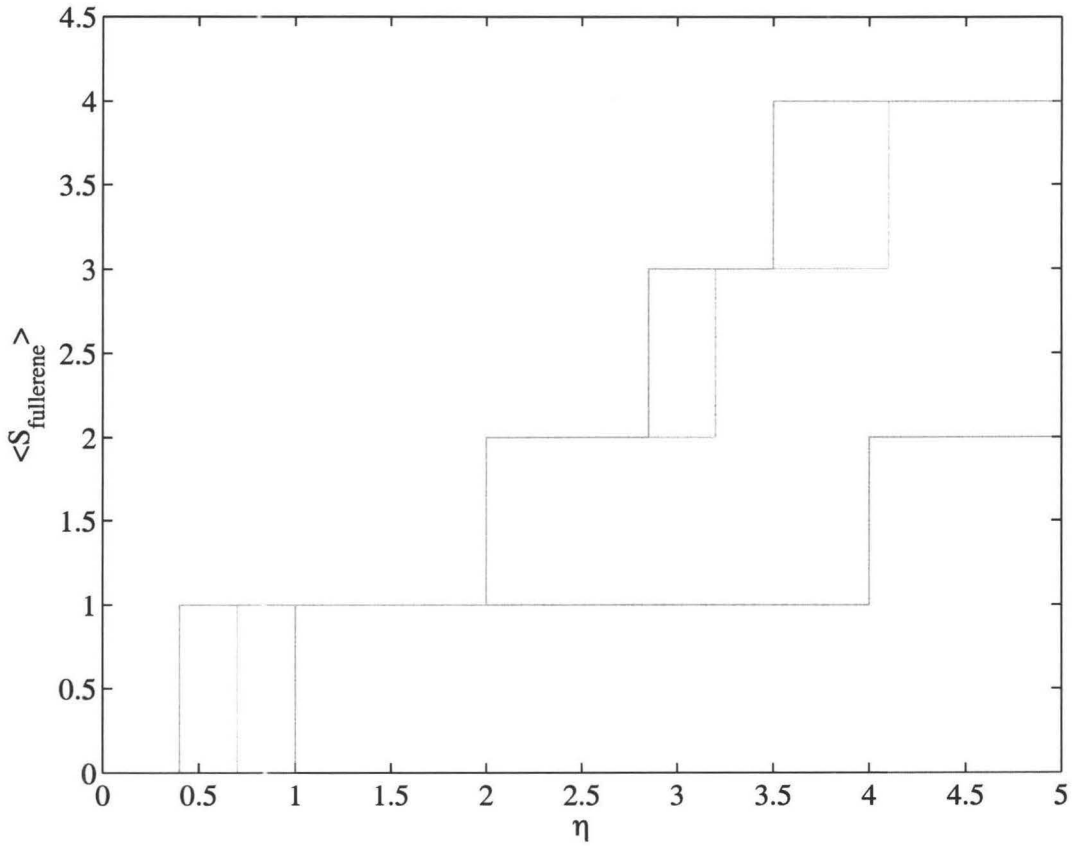

Figure 3.10: $S_{fullerene}$ as a function of the coupling between the cage and the qubit (η). **blue: 4-site ring. green: C_{12} red: 12-site ring.**

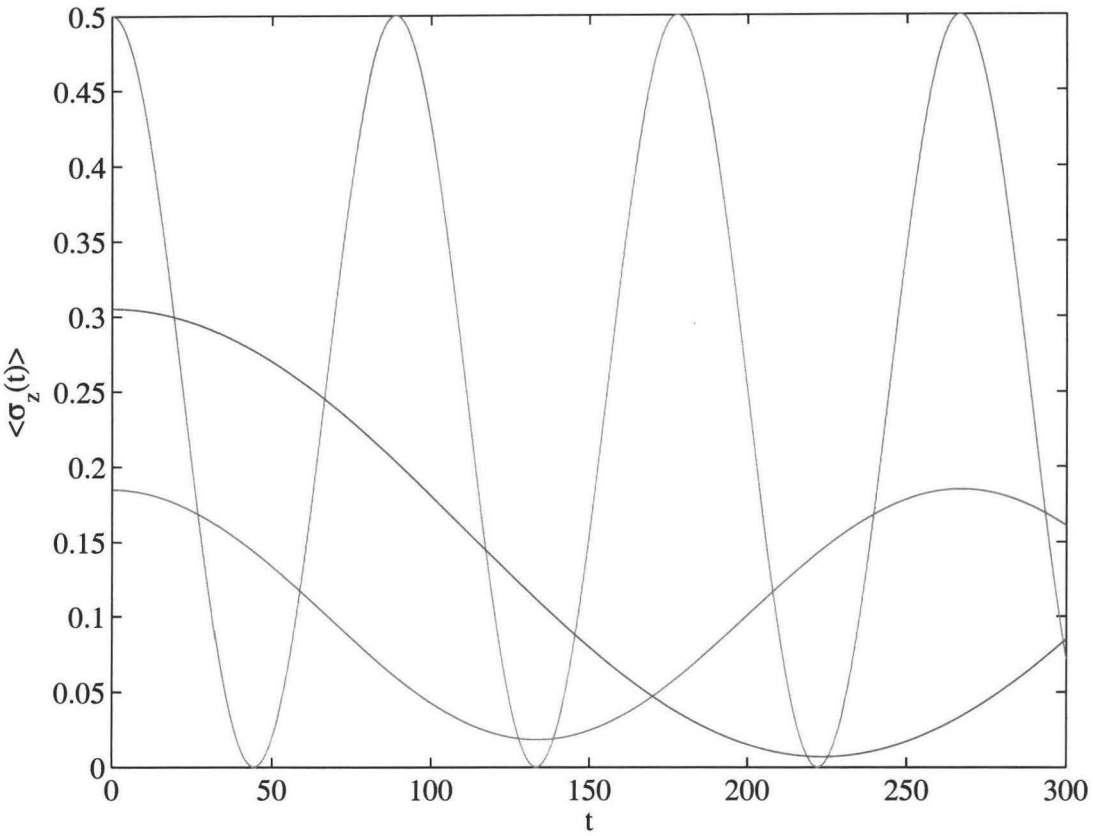

Figure 3.11: Oscillations of $\langle \sigma_z(t) \rangle$ on endohedral doped C_{20}. **green:** $\eta = 0.5$, $B_z = 0.1$, $B_x = 0.1$, $n_{evr} = 500$, $A = 4.738358 \times 10^{-6}$ **red:** $\eta = 0.8$, $B_z = 0.1$, $B_x = 0.1$, $n_{evr} = 500$, $A = 1.922118 \times 10^{-2}$ **yellow:** $\eta = 1.8$, $B_z = 0.1$, $B_x = 0.1$. **5.171604e-03 blue:** $\eta = 1.3$, $B_z = 0.1$, $B_x = 0.1$, $A = 7.137485 \times 10^{-3}$.

The oscillations of the the $\eta = 0.8$ state on the 12-site ring are the same as the oscillations for the $\eta = 0.8$ state on C_{12}. A qubit coupled to C_{12} perturbs the ground state of system for $\eta > 0.8$ when $B_z = 0.1J$ and $B_x = 0.1J$ (Figure 3.2.2). That the dopant perturbs the electronic ground state for $\eta = 0.8$ in C_{12} and $\eta = 0.4$ in the 12-site ring suggests the geometry of C_{12} has a protective effect on the coherence of the qubit.

In C_{20}, the transition from an $S_{fullerene} = 0$ ground state to an $S_{fullerene} = 1$ ground state occurs for $0.5 < \eta < 0.7$. As in C_{12}, the qubit oscillates with a frequency dictated entirely by the external fields for small values of η.

The basis for $\eta = 0.8$ and $\eta = 1.3$ is not sufficiently complete to confirm the presence or absence of high frequency oscillations observed in smaller systems. The maximum amplitude of the missing states is $A = 1.922118 \times 10^{-2}$ for $\eta = 0.8$ and $A = 7.137485 \times 10^{-3}$ for $\eta = 1.3$. As in C_{12}, continuing to increase the coupling past the critical value suppresses the maximum amplitude of any possible high-frequency oscillations.

The amplitude of the qubit oscillations is not initially the maximum value of 0.5 for larger values of η because the "spin down" state is a compromise between aligning the qubit with the external field and minimizing the exchange energy from the coupling of the dopant to the fullerene cage. The period is also modified as the coupling between the fullerene and the qubit changes both the ground state and the splitting between the dopant spin-up and the dopant spin-down components of the ground state.

3.3 Variations on the Hamiltonian

The previous sections investigated the precession of the qubit in the case where the qubit moment was substantially larger than the electron moments on the fullerene - in this case the external fields effectively act only on the qubit. However, for the case where the external fields act on all the sites in the lattice (Eq. 2.15) the total S_z of the system will evolve non-trivially when the magnetic moment of the qubit differs substantially from the magnetic moment of the spins on the fullerene.

The system is initialized with a static B_z field applied to all the spins. Applying a microwave frequency B_x field at the resonance frequency of the electrons in the fullerene effectively switches off the B_z field on the spins (Eq. 2.15); the total $\langle S_z(t) \rangle$ of the systems is then observed as the spins precess in B_x.

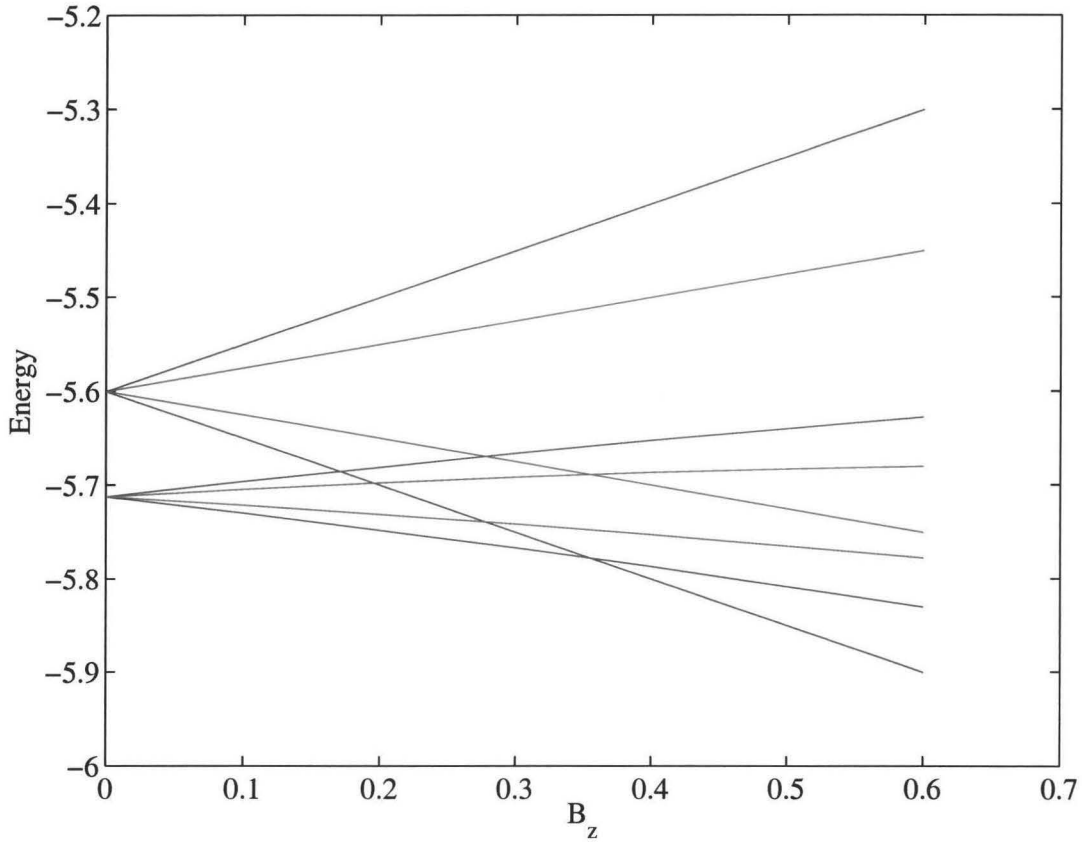

Figure 3.12: Low energy states of C_{12} as a function of the B_z magnetic field, $\eta = 0.8$. **red: Energy for $\mu_e/\mu_Q = 0$ (Hamiltonian from Eq. 2.11). blue Energy for $\mu_e/\mu_Q = 0.5$ (Hamiltonian from Eq. 2.15).**

For the case where the magnetic moment of the dopant is equal to the magnetic moment of the fullerene electrons there is no mixing in the states and $\langle S_z(t) \rangle$ is a cosine. As the qubit moment is varied, states with other energies become accessible and additional low-amplitude oscillations are admitted. However, these oscillations are only readily apparent for very large differences in the moments of the fullerene and qubit spins.

The low energy states evolve linearly as a function of B_z. The rate at which the gap between the qubit spin up and qubit spin down states increases depends on the value of the total fullerene spin (Fig. 3.12).

Chapter 4

Conclusions

The Lanczos algorithm has been implemented on parallel processers to compute the low-energy states of endohedral doped fullerenes under the Heisenberg Hamiltonian. This simple model of a fullerene qubit is used to probe the behaviour of the dopant spin as it precesses in external magnetic fields. A bit-flip operation in which the qubit is aligned either parallel or antiparallel to the external field is modeled by placing the system in the lowest-energy state in the presence of a static B_z field; an oscillating B_x magnetic field causes the dopant spin to precess and the spin of the qubit, $\langle \sigma_z(t) \rangle$, is observed.

For small B_z magnetic fields and weak coupling between the fullerene and dopant, the ground state of the fullerene is unperturbed by the dopant and only the two lowest-energy states are accessible to the precessing dopant. The frequency of the resulting oscillations of $\langle \sigma_z(t) \rangle$ depends only on the magnitude of the external fields, B_z and B_x.

When the coupling between the qubit and the system is increased past a critical value, the ground state of the system is perturbed and $S_{fullerene} \neq 0$. When the system is excited by the application of a B_x field to the qubit, the qubit may relax by releasing energy into the fullerene. This leads to a non-trivial high-frequency oscillations in $\langle \sigma_z(t) \rangle$. Coupling the qubit to the fullerene forces the energy reduction obtained by aligning the dopant with the external static field (B_z) to compete with the minimization of the exchange

energy between the dopant and the fullerene. This reduces the maximum amplitude of $\langle \sigma_z(t) \rangle$ and may also change the frequency at which the bit precesses in C_{20}.

4.1 Further work

The toy model of an endohedral fullerene qubit may be extended in several interesting ways:

- Adding additional spin levels to the dopant increases the resemblance of the system to nitrogen-doped endohedral fullerenes - nitrogen has an electron spin of 3/2 - and the relaxation of the system would be modelled more completely on a four-level spin ladder.

- Coupling the qubit-fullerene system to a bath of harmonic oscillators allows dissipative effects to be described [12].

- Coupling a nuclear spin to the dopant electron allows the relaxation processes of the nuclear qubit to be probed. This calculation would require treating the hyperfine interaction and the spatial part of the wave-function by introducing a term to the Hamiltonian of the form $A(r)(I \cdot S)$ [22] [21]. Because $A(r)$ is spatially dependent, this would require extending the spin part of the fullerene-qubit wave function to include a description of the spatial part of the fullerene-qubit state.

Bibliography

[1] A Ardavan, M Austwick, SC Benjamin, GA Briggs, T Dennis, A Ferguson, DG Hasko, M Kanai, AN Khlobystov, BW Lovett, G Morley, RA Oliver, DG Pettifor, K Porfyrakis, JH Reina, JH Rice, JD Smith, r RA Taylo, A Williams D, C Adelmann, H Mariette, and RJ Hamers. Nanoscale solid-state quantum computing. *Philos. Trans. R. Soc. Lond. Ser. A-Math. Phys. Eng. Sci.*, 361(1808):1473, 2003.

[2] A. Auerbach. *Interacting Electrons and Quantum Magnetism.* Springe, New York, 1994.

[3] Satish Balay, Kris Buschelman, William D. Gropp, Dinesh Kaushik, Matthew G. Knepley, Lois Curfman McInnes, Barry F. Smith, and Hong Zhang. PETSc Web page, 2001. http://www.mcs.anl.gov/petsc.

[4] DS Bethune, RD Johnson, JR Salem, MS de Vries, and CS Yannon. Atoms in carbon cages: the structure and properties of endohedral fullerenes. *Nature*, 366:123 – 128, 1993.

[5] J.K. Callum and Ralph A. Willoughby. *Lanczos algorithms for large symmetric eigenvalue computations: Vol. I: theory.* Birkhauser, Boston, 1985.

[6] Francois Diederich, Roland Ettl, Yves Rubin, Robert L. Whetten, Marcos Beck, Rainer; Alvarez, Samir Anz, Dilip Sensharma, Fred Wudl, Kishan C. Khemani, and Andrew Koch. The higher fullerenes: Isolation and characterization of c76, c84, c90, c94, and c70o, and oxide of d5h-c7. *Science*, 252:548–55, 1991.

[7] David DiVincenzo. The physical implementation of quantum computation. *Fortschritte der Physik*, 48:771, 2000.

[8] M.S. Dresselhaus. *Science of fullerenes and carbon nanotubes.* Academic Press, San Diego, 1996.

[9] W. Harneit. Fullerene-based electron-spin quantum computer. *Phys. Rev. A*, 65(3):032322, 2002.

[10] M. Karbach and G. Muller. Introduction to the bethe ansatz i. http://arxiv.org/cond-mat/9809162.

[11] N.P. Konstantinidis. The antiferromagnetic heisenberg model on clusters of fullerene type symmetry. available on arxiv.

[12] A.J. Legget, S. Chakravarty, AT Dorsey, MPA Fisher, A. Garg, and W. Zwergert. Dynamics of the dissipative two-state system. *Reviews of Modern Physics*, 59:1, 1987.

[13] R. B. Lehoucq, D. C. Sorensen, and C. Yang. Arpack, 1997. http://www.caam.rice.edu/software/ARPACK/.

[14] R. Lopez-Sandoval. Electron correlations in a c_{20} fullerene cluster: A lattice density-functional study of the hubbard model. *The European Physical Journal D*, 38:507–514, 2006.

[15] Harald Mauser. Stabilization of atomic nitrogen inside c60. *Angewandte Chemie, International Edition in English*, 36(24):2835–2838, 1997.

[16] N.A. Modine and Efthimios Kaxiras. Variational hilbert space truncation approach to quantum heisenberg antiferromagnets on frustrated clusters. *Phys Rev B*, 53:2546, 1996.

[17] J.L. Morton. *Electron Spins In Fullerenes As Prospective Qubits.* PhD thesis, Oxford, 2005.

[18] John J. L. Morton. Electron spin relation of $N@C_{60}$ in CS_2. *J. Chem. Phys*, 124:014508, 2006.

[19] John J.L. Morton, Alexei M. Tyryshkin, Arzhang Ardavan, Kyriakos Porfyrakis, Stephen A. Lyon, G. Andrew, and D. Briggs. A new mechanism for electron spin echo envelope modulation. *J. Chem. Phys*, 122:174504, 2005.

[20] Horst Prinzbach, Andreas Weiler, Peter Landenberger, Fabian Wahl, Jrgen Wrth, Lawrence T. Scott, Marc Gelmont, Daniela Olevano, and Bernd v. Issendorff. Gas-phase production and photoelectron spectroscopy of the smallest fullerene, c20. *Nature*, 407:60–63, 2000.

[21] D. D. Bhaktavatsala Rao, V. Ravishankar, and V. Subrahmanyam. Spin decoherence from hamiltonian dynamics in quantum dots. accepted for publication in Phys.Rev A, http://arxiv.org/abs/quant-ph/0602027.

[22] N. Sahoo, S.B. Sulaiman, K.C. Mishra, and T.P. Das. Theory of structure and hyperfine properties of anomalous muonium in elemental semiconductors: Diamond, silicon, and germanium. *Phys Rev B*, 39:13389–13410, 1989.

[23] Lorenza Viola and Seth Lloyd. Dynamical suppression of decoherence in two-state quantum systems. *Phys. Rev. A*, 58:2733, 1998.

[24] Xiaoqing Yu, Congjun Wu, Chui-Lin Wang, and Zhao-Bin . Su. Electronic and structural properties of c_{36} molecule. *Int. J. Mod. Phys. B*, 13:1513, 1999.

Low-energy spectra for bare fullerenes

Table 1: Low Energy States of C_{12} calculated with the Lanczos routine

State energy (units of J)	State energy per site (units of J)	$\|\|H\psi - E\psi\|\|$	S^2
-5.700913312923364	-0.475076109410280	0.000000000000630	-0.000000000000000
-5.013103134044950	-0.417758594503746	0.000000000618162	1.999999999999994
-5.013103134044950	-0.417758594503746	0.000000000000733	2.000000000000000
-5.013103134044950	-0.417758594503746	0.000000000000000	2.000000000000000
-5.013103134044950	-0.417758594503746	0.000000000002230	1.999999999999996
-5.013103134044950	-0.417758594503746	0.000000000085096	2.000000000000002
-5.013103134044949	-0.417758594503746	0.000000000217673	2.000000000000000
-5.013103134044949	-0.417758594503746	0.000000000061601	1.999999999999997
-5.013103134044949	-0.417758594503746	0.000000000000000	1.999999999999999
-5.013103134044947	-0.417758594503746	0.000000002201200	2.000000000000005
-4.805169381152931	-0.400430781762744	0.000000000008178	-0.000000000000000
-4.805169381152931	-0.400430781762744	0.000000000000003	-0.000000000000000
-4.670620565159545	-0.389218380429962	0.000000000009471	-0.000000000000000
-4.670620565159545	-0.389218380429962	0.000000000000396	-0.000000000000000
-4.670620565159533	-0.389218380429961	0.000000003538644	0.000000000000034
-4.657885305020255	-0.388157108751688	0.000000000005391	2.000000000000000
-4.657885305020253	-0.388157108751688	0.000000000000375	1.999999999999991
-4.657885305020253	-0.388157108751688	0.000000000010153	1.999999999999997
-4.657885305020253	-0.388157108751688	0.000000001067907	1.999999999999996
-4.322917182968258	-0.360243098580688	0.000000000578139	2.000000000000000
-4.322917182968258	-0.360243098580688	0.000000000037373	1.999999999999997
-4.322917182968258	-0.360243098580688	0.000000000099228	2.000000000000005
-4.322917182968235	-0.360243098580686	0.000000003614014	1.999999999999980
-4.181508284786400	-0.348459023732200	0.000000000000902	-5.0.000000000000000

Table 2: Low Energy States of C_{12} calculated with LAPACK

State energy (units of J)	State energy per site (units of J)	$\|\|H\psi - E\psi\|\|$	S^2
-5.700913312923364	-0.475076109410280	0.000000000000000	0.000000000000000
-5.013103134044954	-0.417758594503746	0.000000000000000	2.000000000000004
-5.013103134044950	-0.417758594503746	0.000000000000000	2.000000000000001
-5.013103134044950	-0.417758594503746	0.000000000000000	2.000000000000004
-5.013103134044950	-0.417758594503746	0.000000000000000	1.999999999999999
-5.013103134044950	-0.417758594503746	0.000000000000000	2.000000000000002
-5.013103134044950	-0.417758594503746	0.000000000000000	1.999999999999998
-5.013103134044950	-0.417758594503746	0.000000000000000	2.000000000000007
-5.013103134044947	-0.417758594503746	0.000000000000000	1.999999999999999
-5.013103134044943	-0.417758594503745	0.000000000000000	2.000000000000003
-4.805169381152933	-0.400430781762744	0.000000000000000	0.000000000000000
-4.805169381152929	-0.400430781762744	0.000000000000000	-0.000000000000000
-4.670620565159549	-0.389218380429962	0.000000000000000	0.000000000000000
-4.670620565159545	-0.389218380429962	0.000000000000000	-0.000000000000000
-4.670620565159545	-0.389218380429962	0.000000000000000	-0.000000000000000
-4.657885305020258	-0.388157108751688	0.000000000000000	2.000000000000003
-4.657885305020255	-0.388157108751688	0.000000000000000	2.000000000000002
-4.657885305020255	-0.388157108751688	0.000000000000000	2.000000000000004
-4.657885305020255	-0.388157108751688	0.000000000000000	2.000000000000001
-4.657885305020255	-0.388157108751688	0.000000000000000	2.000000000000001
-4.657885305020255	-0.388157108751688	0.000000000000000	2.000000000000004
-4.657885305020255	-0.388157108751688	0.000000000000000	2.000000000000000
-4.657885305020255	-0.388157108751688	0.000000000000000	2.000000000000004
-4.322917182968260	-0.360243098580688	0.000000000000000	2.000000000000001
-4.322917182968260	-0.360243098580688	0.000000000000000	2.000000000000001
-4.322917182968260	-0.360243098580688	0.000000000000000	2.000000000000004
-4.322917182968260	-0.360243098580688	0.000000000000000	2.000000000000008
-4.322917182968260	-0.360243098580688	0.000000000000000	1.999999999999997
-4.322917182968260	-0.360243098580688	0.000000000000000	2.000000000000001
-4.322917182968260	-0.360243098580688	0.000000000000000	2.000000000000004
-4.322917182968256	-0.360243098580688	0.000000000000000	1.999999999999998
-4.322917182968256	-0.360243098580688	0.000000000000000	2.000000000000005
-4.181508284786400	-0.348459023732200	0.000000000000000	0.000000000000000

Table 3: Low Energy States of C_{20}

State energy (units of J)	State energy per site (units of J)	$\|\|H\psi - E\psi\|\|$	S^2
-9.722185349763754	-0.486109267488188	0.000000000000024	0.000000014491804
-9.406514829554100	-0.470325741477705	0.000000000003814	0.000000008251043
-9.406514829554100	-0.470325741477705	0.000000000000262	0.000000010046114
-9.406514829554096	-0.470325741477705	0.000000000361484	0.000000197328836
-9.406514829554093	-0.470325741477705	0.000000000657890	0.000000271301725
-9.406514829554027	-0.470325741477701	0.000000002181280	0.000000464751536
-9.352363195494219	-0.467618159774711	0.000000001728760	0.000000543577507
-9.208359045143972	-0.460417952257199	0.000000000565857	1.999999999999970
-9.208359045143949	-0.460417952257197	0.000000001393547	1.999999999999982
-9.208359045143878	-0.460417952257194	0.000000002179739	1.999999999999988
-9.186487641575109	-0.459324382078755	0.000000000284664	1.999999999999998
-9.186487641575107	-0.459324382078755	0.000000000159090	2.000000000000018
-9.186487641575104	-0.459324382078755	0.000000000554801	2.000000000000014
-9.186487641575050	-0.459324382078753	0.000000001690173	2.000000000000000
-9.130477300221186	-0.456523865011059	0.000000000266565	1.999999999999962
-9.130477300221161	-0.456523865011058	0.000000000101937	1.999999999999990
-9.130477300221155	-0.456523865011058	0.000000000534814	1.999999999999992
-8.971119446282625	-0.448555972314131	0.000000000715763	1.999999999999974
-8.971119446282584	-0.448555972314129	0.000000000194269	1.999999999999988
-8.971119446282563	-0.448555972314128	0.000000000247149	1.999999999999753
-8.879640181632722	-0.443982009081636	0.000000000792759	0.000000253816170
-8.879640181632675	-0.443982009081634	0.000000000509498	0.000000198914314
-8.879640181632672	-0.443982009081634	0.000000000554260	0.000000335704361
-8.879640181632627	-0.443982009081631	0.000000002434067	0.000001329390839

Table 4: Low Energy States of C_{24}

State energy (units of J)	State energy per site (units of J)	$\|\|H\psi - E\psi\|\|$	S^2
-11.719373047017649	-0.488307210292402	0.000000000143871	0.000000071579316
-11.704784243166921	-0.487699343465288	0.000000001684887	0.000000385525891
-11.468142211171918	-0.477839258798830	0.000000000047479	2.000000000000007
-11.468142211171143	-0.477839258798798	0.000000003211561	1.999999999998867
-11.372435589722327	-0.473851482905097	0.000000001179445	1.999999999999859
-11.297791397867531	-0.470741308244480	0.000000002765740	0.000008235464610
-11.293257169962208	-0.470552382081759	0.000000000762243	0.000002435591321
-11.293257169957487	-0.470552382081562	0.000000001369766	0.000004513269438
-11.278884360063566	-0.469953515002649	0.000000001638095	1.999999999999178
-11.263405293513632	-0.469308553896401	0.000000001252567	1.999999999999851
-11.263405293513481	-0.469308553896395	0.000000001891064	1.999999999940207
-11.245651121913435	-0.468568796746393	0.000000003033786	0.000019989213297
-11.245651121912896	-0.468568796746371	0.000000003826555	0.000015273794249
-11.236519279622957	-0.468188303317623	0.000000002015424	2.000000000000004
-11.236519279618788	-0.468188303317449	0.000000003276825	1.999999999121036
-11.230427585713004	-0.467934482738042	0.000000000674189	0.000055276346361
-11.228516533088200	-0.467854855545342	0.000000000226880	1.999999999999961
-11.228516533087394	-0.467854855545308	0.000000004166523	1.999999999997882
-11.178826163258806	-0.465784423469117	0.000000003007327	1.999999999959881
-11.178826163258298	-0.465784423469096	0.000000002823945	1.999999999958438
-11.164366575833407	-0.465181940659725	0.000000002725366	0.000002145961714
-11.164366575830504	-0.465181940659604	0.000000003711514	0.000001950228376
-11.162573351349051	-0.465107222972877	0.000000000480260	0.000000057556499
-11.162573351347563	-0.465107222972815	0.000000001288563	0.000017577683826

Table 5: Low Energy States of C_{26}

State energy (units of J)	State energy per site (units of J)	$\|\|H\psi - E\psi\|\|$	S^2
-12.608975987183889	-0.484960614891688	0.000000000419195	0.000000202999151
-12.557386043648165	-0.482976386294160	0.000000000353562	0.000000190990472
-12.557386043648005	-0.482976386294154	0.000000001145814	0.000000952245013
-12.492973367580371	-0.480498975676168	0.000000000243774	1.999999999999742
-12.492973367580172	-0.480498975676160	0.000000000834040	1.999999999996209
-12.461743788704164	-0.479297838027083	0.000000001267930	0.000004603999508
-12.448616490673372	-0.478792941948976	0.000000000749644	0.000000821738797
-12.426818450064578	-0.477954555771715	0.000000003326034	0.000020705790943
-12.426818450057063	-0.477954555771425	0.000000002171985	0.000081790617682
-12.421292450721124	-0.477742017335428	0.000000001943563	1.999999998326529
-12.421292450710572	-0.477742017335022	0.000000003028183	1.999999999895969
-12.382166458861130	-0.476237171494659	0.000000000681692	1.999999999999963
-12.378886647525682	-0.476111024904834	0.000000000376492	1.999999999996627
-12.315019231597624	-0.473654585830678	0.000000002189100	0.000032171838123
-12.305771070438322	-0.473298887324551	0.000000001267353	1.999999999744132
-12.305771070436242	-0.473298887324471	0.000000002294212	1.999999999999742
-12.288844734818625	-0.472647874416101	0.000000000417189	1.999999999997749
-12.288844734817866	-0.472647874416072	0.000000001230590	1.999999999987169
-12.263751320298086	-0.471682743088388	0.000000000912133	0.000008165937410
-12.263751320297118	-0.471682743088351	0.000000000652957	0.000001247032614
-12.210568343034655	-0.469637243962871	0.000000001763322	1.999999999996666
-12.161920207330084	-0.467766161820388	0.000000002763768	1.999999999884085
-12.161920207328768	-0.467766161820337	0.000000002982777	1.999999999996568
-12.151825146558178	-0.467377890252238	0.000000003027982	0.000069211211851

Table 6: Low Energy States of C_{28} td isomer

State energy (units of J)	State energy per site (units of J)	$\|\|H\psi - E\psi\|\|$	S^2
-13.574863542880509	-0.484816555102875	0.000000002789311	0.000004263396923
-13.574863542879095	-0.484816555102825	0.000000001968432	0.000023329797742
-13.559781051009574	-0.484277894678913	0.000000001716218	1.999999999861419

Table 7: C_{28} d2 isomer

State energy (units of J) (units of J)	State energy per site (units of J)	$\|\|H\psi - E\psi\|\|$	S^2
-13.860224786030559	-0.495008028072520	0.000000000027107	0.000000014727005
-13.657531071302238	-0.487768966832223	0.000000003157063	0.000010166336598
-13.605307275073681	-0.485903831252631	0.000000001054179	1.999999999985666

Table 8: 10 site ring, $\eta = 1.05$, $B_z = 0.0$, $B_x = 0.0$ - in this case S^2 is a good quantum number for the Hamiltonian (Eq. 2.15)

State energy (units of J)	State energy per site (units of J)	$\|\|H\psi - E\psi\|\|$	S^2
-5.010957346738667	-0.455541576976242	0.000000003000625	0.750000000000007
-5.010957346738667	-0.455541576976242	0.000000000000000	0.750000000000000
-4.462029374312694	-0.405639034028427	0.000000000939293	0.750000000000001
-4.462029374312692	-0.405639034028427	0.000000000000006	0.749999999999998
-4.462029374312692	-0.405639034028427	0.000000000000164	0.750000000000000
-4.419681869054436	-0.401789260823131	0.000000000000024	3.750000000000001
-4.419681869054436	-0.401789260823131	0.000000000149968	3.749999999999993
-4.419681869054434	-0.401789260823130	0.000000000013154	3.750000000000000

Table 9: 10 site ring, $\eta = 1.05$, $B_z = 0.0$, $B_x = 0.1$ in this case S^2 is not a good quantum number for the Hamiltonian (Eq. 2.15)

State energy (units of J)	State energy per site (units of J)	$\|\|H\psi - E\psi\|\|$	S^2
-5.019639643703377	-0.456330876700307	0.000000000736889	0.750657444529246
-5.002980438122110	-0.454816403465646	0.000000000098143	0.750685851500572
-4.470711671277401	-0.406428333752491	0.000000000000004	0.750657444217310
-4.470711671277400	-0.406428333752491	0.000000000000324	0.750657444217309
-4.454052465696135	-0.404913860517830	0.000000000001051	0.750685851491862
-4.454052465696135	-0.404913860517830	0.000000000000000	0.750685851491859
-4.434832519639899	-0.403166592694536	0.000000000000000	3.750283678890563
-4.424909553365575	-0.402264504851416	0.000000000000002	3.750431963891041
-4.414911294432637	-0.401355572221149	0.000000000000000	3.750438594891565

Table 10: 10 site ring, $\eta = 0.1$, $B_z = 0.0$, $B_x = 0.1$ in this case S^2 is not a good quantum number for lowest energy state of the Hamiltonian (Eq. 2.15). η is below the critical value, the lowest energy state is not a mixture of states with different spins.

State energy (units of J)	State energy per site (units of J)	$\|\|H\psi - E\psi\|\|$	S^2
-4.527946354492045	-0.411631486772004	0.000000000000000	0.750000000000004
-4.477946354492044	-0.407086032226549	0.000000000001666	0.750000000000000
-4.191309887117111	-0.381028171556101	0.000000000000000	0.806624327025938
-4.175418024857322	-0.379583456805211	0.000000000000000	0.835786437626906
-4.054707346738667	-0.368609758794424	0.000000000000789	3.750000000000001
-4.033996668620011	-0.366726969874546	0.000000000012281	3.664213562065423
-4.018104806360222	-0.365282255123657	0.000000000045459	3.693375675032213
-4.004707346738666	-0.364064304248970	0.000000000035497	3.750000000000006
-3.783097435408445	-0.343917948673495	0.000000000003425	0.750000000000000

Table 11: 4 site ring, $\eta = 1.1$, State prepared with $B_z = 0.1$ on/off, $B_x = 0.1$ off/on

State energy (units of J)	S^2_{system}	$S^2_{fullerene}$
-1.979506731918409	0.750624349662844	2.000000000000000
-1.946166600026652	0.750599640239832	2.000000000000000
-1.912500000000000	0.750000000000000	0.000000000000000
-1.812500000000000	0.750000000000000	-0.000000000000000
-0.979506731918409	0.750624349662844	2.000000000000000

Table 12: 4 site ring, $\eta = 0.1$, State prepared with $B_z = 0.1$ on/off, $B_x = 0.1$ off/on, $\mu_{qubit} = 2\mu_{fullerene}$

State energy (units of J)	S^2_{system}	$S^2_{fullerene}$
-2.037500000000001	0.750000000000000	0.000000000000000
-1.937500000000000	0.750000000000000	-0.000000000000000
-1.108210678118655	0.835786437626904	2.000000000000000
-1.074102540378445	0.806624327025936	2.000000000000000
-1.037500000000000	3.749999999999998	1.999999999999999
-0.966789321881345	3.664213562373093	1.999999999999999